A Cathepsin-Targeted Quenched Activity–Based Probe Facilitates Enhanced Detection of Human Tumors during Resection

Gregory T. Kennedy[1], David E. Holt[2], Feredun S. Azari[1], Elizabeth Bernstein[1], Bilal Nadeem[1], Ashley Chang[1], Neil T. Sullivan[1], Alix Segil[1], Charuhas Desphande[3], Eric Bensen[4], John T. Santini Jr[4], John C. Kucharczuk[1], Edward J. Delikatny[5], Matthew Bogyo[6], A.J. Matthew Egan[7], Charles W. Bradley[8], Evgeniy Eruslanov[1], Jason D. Lickliter[9], Gavin Wright[10,11], and Sunil Singhal[1]

ABSTRACT

Purpose: Fluorescence-guided surgery using tumor-targeted contrast agents has been developed to improve the completeness of oncologic resections. Quenched activity–based probes that fluoresce after covalently binding to tumor-specific enzymes have been proposed to improve specificity, but none have been tested in humans. Here, we report the successful clinical translation of a cathepsin activity–based probe (VGT-309) for fluorescence-guided surgery.

Experimental Design: We optimized the specificity, dosing, and timing of VGT-309 in preclinical models of lung cancer. To evaluate clinical feasibility, we conducted a canine study of VGT-309 during pulmonary tumor resection. We then conducted a randomized, double-blind, dose-escalation study in healthy human volunteers receiving VGT-309 to evaluate safety. Finally, we tested VGT-309 in humans undergoing lung cancer surgery.

Results: In preclinical models, we found highly specific tumor cell labeling that was blocked by a broad spectrum cathepsin inhibitor. When evaluating VGT-309 for guidance during resection of canine tumors, we found that the probe selectively labeled tumors and demonstrated high tumor-to-background ratio (TBR; range: 2.15–3.71). In the Phase I human study, we found that VGT-309 was safe at all doses studied. In the ongoing Phase II trial, we report two cases in which VGT-309 localized visually occult, non-palpable tumors (TBRs = 2.83 and 7.18) in real time to illustrate its successful clinical translation and potential to improve surgical management.

Conclusions: This first-in-human study demonstrates the safety and feasibility of VGT-309 to label human pulmonary tumors during resection. These results may be generalizable to other cancers due to cathepsin overexpression in many solid tumors.

Introduction

The mainstay of therapy for most solid tumors is surgical resection, but many tumors recur locally after curative-intent resection due to the microscopic presence of malignant cells missed at the index operation (1). Thus, there is a pressing, unmet need for a real-time method to improve surgeons' ability to identify the extent of malignancy during resection. A particularly attractive approach to this clinical problem is intraoperative molecular imaging (IMI), a technology that involves delivering tumor-targeted optical contrast agents to cancer cells and detecting them with wavelength-specific camera systems (2).

Recently, there has been interest in developing "smart" optical probes to highlight tumors in a highly selective manner that reduces background, off target fluorescence (3–5). These tracers become fluorescent after processing by an enzyme or in response to a physiologic change common to different cancer types or tumor microenvironments (6–9). Within the family of smart optical probes are quenched activity–based probes (qABP), small molecules that modify a defined set of enzyme targets on the basis of their ability to form specific covalent bonds with catalytic residues (10). This mechanism-based labeling reaction has been used as a tool to dissect key biological functions of proteases in cellular and animal models of disease, but has only recently been optimized for systemic delivery and detection of cancer cells (11).

A promising enzyme target family for qABP imaging of cancer is the cysteine cathepsins (12). Cysteine cathepsins are a class of proteases that have established functions as enzymes of the lysosomal degradation system, but are now known to have a range of extra-lysosomal functions (13). Certain normal tissues express cathepsins, including the kidney, thymus, spleen, and liver (14). Cathepsin protease activity is frequently dysregulated in the context of neoplastic transformation. Increased activity and aberrant localization of cysteine cathepsins within the tumor microenvironment have a potent role in driving cancer progression, proliferation, invasion, and metastasis (15). Cathepsins are overexpressed in many diverse cell types within tumors including cancer cells and tumor-associated macrophages (TAM; ref. 13). Cysteine cathepsins are also often secreted into the extracellular space

[1]Department of Surgery, University of Pennsylvania School of Medicine, Philadelphia, Pennsylvania. [2]Department of Clinical Sciences and Advanced Medicine, University of Pennsylvania School of Veterinary Medicine, Philadelphia, Pennsylvania. [3]Department of Pathology, University of Pennsylvania School of Medicine, Philadelphia, Pennsylvania. [4]Vergent Bioscience, Minneapolis, Minnesota. [5]Department of Radiology, University of Pennsylvania School of Medicine, Philadelphia, Pennsylvania. [6]Department of Pathology, Stanford University, Palo Alto, California. [7]Department of Pathology, St. Vincent's Hospital, Melbourne, Australia. [8]Department of Pathobiology, University of Pennsylvania School of Veterinary Medicine, Philadelphia, Pennsylvania. [9]Nucleus Network, Melbourne, Australia. [10]Department of Surgery, St. Vincent's Hospital, University of Melbourne, Melbourne, Australia. [11]Victorian Comprehensive Cancer Centre Alliance, Melbourne, Australia.

Corresponding Author: Sunil Singhal, Department of Surgery, University of Pennsylvania Perelman School of Medicine, 3400 Civic Center Boulevard, 14th Floor, South Pavillion, Philadelphia, PA 19104. Phone: 215-298-4998; E-mail: sunil.singhal@pennmedicine.upenn.edu

Clin Cancer Res 2022;28:3729–41

doi: 10.1158/1078-0432.CCR-22-1215

Translational Relevance

We report a comprehensive preclinical evaluation and the first-in-human testing of a cathepsin activity–based probe (VGT-309) for the intraoperative imaging of lung cancer. We demonstrate the safety and feasibility of VGT-309 for localizing visually occult, non-palpable tumors in real time during surgery. These results may be generalizable to other cancers due to cathepsin overexpression in many tumor types.

within the tumor microenvironment where they play roles in promoting tumor cell migration and angiogenesis (15). Inhibitors of cysteine cathepsins have garnered interest as novel cancer therapies, due to preclinical evidence suggesting limited off-target effects with a substantial therapeutic index (14). Targeting cathepsins for cancer imaging is also an attractive strategy given that virtually all solid tumors contain elevated levels of these proteases (13).

In this study, we evaluated VGT-309, a cathepsin-targeted qABP, for the intraoperative detection of lung cancer during resection. VGT-309 is based upon the parent probe BMV109, which was developed using a Cy5 fluorophore for use in cellular and animal models (16). The probes contain the same phenoxymethyl ketone electrophile that covalently and irreversibly binds active cysteine cathepsins, but in VGT-309, the far-red Cy5 fluorophore is replaced with the near-infrared (NIR) indocyanine green (ICG; **Fig. 1A**; ref. 17). The use of this NIR fluorophore confers two major advantages: (i) significant depth of signal penetration to identify tumors below the organ surface, and (ii) the ability to be detected by FDA-approved, widely available surgical imaging devices.

Here, we report a comprehensive evaluation of VGT-309, including preclinical cellular and animal studies, a Phase I safety trial, and a first-in-human study of the ability of this qABP to localize cancer during resection. We found that VGT-309 selectively labeled tumor cells at both macroscopic and microscopic levels with minimal background fluorescence. In the pilot human study, IMI with VGT-309 allowed the localization of tumors that could not be identified by visual inspection or manual palpation of the lungs. Our study specifically evaluated pulmonary tumors, but the results may be generalizable for a broad range of other cancers due to the demonstrated cathepsin overexpression in the majority of solid tumors.

Materials and Methods

Study drug

VGT-309 (chemical formula $C_{127}H_{142}ClF_4N_{10}Na_3O_{23}S_5$; molecular weight, 2,517.29 Da) is a qABP that consists of a phenoxymethyl ketone electrophile that covalently and irreversibly binds active cysteine cathepsins, coupled to a ICG fluorophore (excitation peak = 789 nm, emission peak = 814 nm) and a IRDye QC-1 quencher (LI-COR Biosciences, Lincoln, NE). Upon binding, the quencher is released to allow NIR fluorescence signal from the probe (**Fig. 1A**). VGT-309 drug substance and drug product were manufactured in compliance with Good Manufacturing Practices by LI-COR Biosciences (Lincoln, NE) and UI Pharmaceuticals (Iowa City, IA), respectively. Vials containing 11 mg of lyophilized VGT-309 drug product were reconstituted with water for injection to a final concentration of 5 mg/mL and diluted with pH 7.4 PBS, culture media, or Baxter Compound Sodium Lactate (Hartmann's) for the appropriate application.

Cell lines

The human cervical carcinoma cell line KB was chosen as a positive control in our experiments, given its previous use as a control in studies of cathepsin expression in human tumors (18, 19). A range of human non–small cell lung cancer (NSCLC) cell lines were obtained from our laboratory or those of collaborators at the University of Pennsylvania. These included A549 (adenocarcinoma), H460 (large cell carcinoma), H513 (adenosquamous cell carcinoma), and H1264 (squamous cell carcinoma). Cell lines were maintained *in vitro* using media containing RPMI, 10% FBS, 2 mmol/L glutamine, and 5 mg/mL penicillin/streptomycin. Cell lines were regularly tested and maintained negative for Mycoplasma spp using MycoAlert Mycoplasma Detection Kit (Lonza).

Western blotting assays

Preparation of whole-cell protein lysates and Western blotting were performed as described previously (20). Briefly, whole-cell protein lysates (50 μg) were electrophoresed through 12% denaturing polyacrylamide slab gels, and the protein bands were transferred to a polymer of vinylidene fluoride (PVDF) membrane (Bio-Rad, Hercules, CA) by electroblotting. Primary antibodies against cathepsins B, L, S, and X (Santa Cruz Biotechnology) were used in our study.

SDS-PAGE analysis of probe-labeled species

To evaluate the binding specificity of VGT-309 to individual cysteine cathepsins as well as the activity dependence of the probe, we conducted fluorescent SDS-PAGE analysis of probe-labeled species using a protocol previously described (21). Briefly, we incubated A549 cells with 1 μmol/L VGT-309 for 2 hours after pretreatment of cells for 30 minutes with 100 μmol/L JPM-OEt (MedChemExpress, Monmouth, NJ), a pan-cathepsin inhibitor. We lysed the cells and loaded lysates and a fluorescent molecular weight maker on an SDS-PAGE gel and ran the gel for 15 minutes at 80 V and subsequently at 130 V until the dye front had run off the gel. Gels were imaged on the Odyssey NIR scanner (LI-COR Biosciences, Lincoln, NE) and individual cathepsin bands were assigned by molecular weight. To control for equal protein loading, gels protein bands were transferred to a PVDF membrane and probed for GAPDH (Santa Cruz Biotechnology) as a loading control.

Evaluation of in vitro binding and internalization of VGT-309 in human lung cancer cells by fluorescence microscopy

According to methods described previously (22), cell lines were cultured on poly-L-lysine—coated glass coverslips in 6-well plates with RPMI media supplemented with 10% FBS, L-Glutamine, and penicillin/streptomycin for 24 hours. For internalization time course studies, cells were treated with 200 nmol/L LysoTracker (Invitrogen, Waltham, MA) for 2 hours prior to incubation with 1 μmol/L VGT-309. Coverslips were removed from culture after varying intervals (5 minutes, 10 minutes, 30 minutes, 60 minutes, 120 minutes, 300 minutes). To examine dose dependence, cells were incubated with different concentrations of VGT-309 (0.01 μmol/L, 0.05 μmol/L, 0.1 μmol/L, 0.5 μmol/L, 1 μmol/L, 5 μmol/L) for 2 hours. For cathepsin-inhibition experiments, cells underwent a 30-minute pretreatment with 100 μmol/L JPM-OEt (MedChemExpress, Monmouth, NJ), a pan-cathepsin inhibitor. Pretreated and non-pretreated cells were then incubated with 1 μmol/L VGT-309 for 2 hours. Following dye administration, coverslips were mounted on glass slides with ProLong Gold antifade reagent with DAPI (Fisher Scientific, Waltham, MA) and imaged on a Leica DM6 B fluorescence microscope (Leica Microsystems, Wetzlar, Germany).

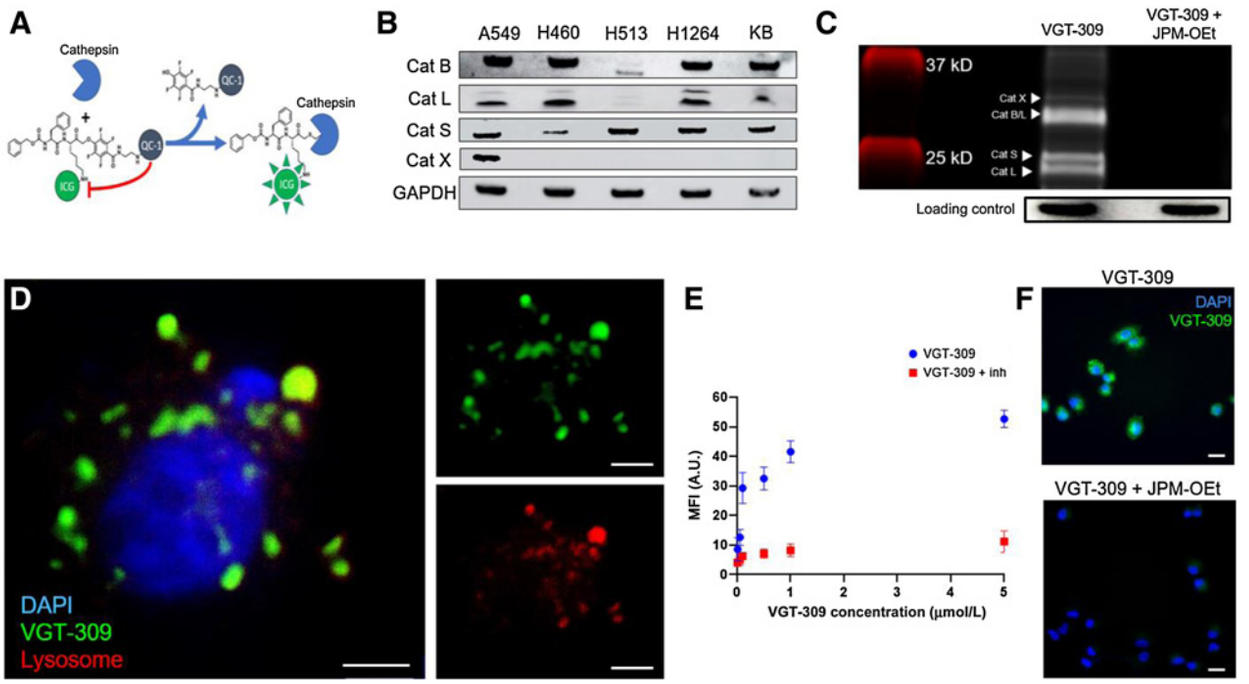

Figure 1.

VGT-309 labels human lung cancer cell lines in a cathepsin activity–dependent manner. **A,** Mechanism of action of VGT-309. The ICG fluorophore is quenched by the QC-1 quencher until it is cleaved upon covalent binding by cysteine cathepsins. **B,** Western blot analysis of cathepsin expression in human NSCLC cell lines with KB (human cervical carcinoma) used as a positive control. **C,** SDS-PAGE analysis of probe-labeled species in H1264 (human pulmonary squamous cell carcinoma) cells with and without pretreatment with 100 μmol/L JPM-OEt, a broad spectrum cathepsin inhibitor. **D,** Fluorescence microscopy of A549 (human pulmonary adenocarcinoma) cells at 100x magnification 1 hour after treatment with 1 μmol/L VGT-309. Cells were co-stained with DAPI and Lyso-Tracker. VGT-309 labeling (shown in green) is predominantly lysosomal (shown in red) in distribution. Overlay images are shown at left with VGT-309 channel and Lyso-Tracker channels shown at right. Scale bars represent 5 μm. **E,** Fluorescence intensity of A549 cells 1 hour after administration of increasing concentrations of VGT-309. Cells were pretreated for 30 minutes with either JPM-OEt or DMSO vehicle prior to VGT-309 administration. **F,** Fluorescence microscopy showing VGT-309 fluorescence in A549 cells with and without pretreatment with JPM-OEt, showing cathepsin-activity dependence of fluorescence. Scale bars represent 20 μm.

Evaluation of in vivo tumor labeling in small animal models

All animal studies were approved by the University of Pennsylvania Institutional Animal Care and Use Committee (IACUC). As described previously (22), female athymic nude mice bearing flank KB xenografts measuring 250 ± 50 mm^3 were randomized to intravenous VGT-309 delivery at 3 dosage levels: 1.0 mg/kg, 2.0 mg/kg, and 4.0 mg/kg ($n = 5$ per dosing level). Dose levels were selected on the basis of the dose of VGT-309 previously shown to label tumors in a murine model of breast cancer (17). After tail vein injection, the fluorescence of tumor and background was recorded at several time points using the Iridium *In Vivo* Imaging System (Vision Sense, New York, NY). VGT-309 fluorescence was obtained using the 800-nm channel, which uses an excitation light source of 785 nm and emission detection at 820 nm. Mean fluorescence of regions of interest (ROI) were delineated over tumor sites and compared with surrounding soft tissue (background) to create a tumor-to-background ratio (TBR). Mice were sacrificed at 24 hours ($n = 3$ per group) and 48 hours ($n = 2$ per group), and organs were harvested and imaged using the Pearl imaging system for biodistribution analysis.

After optimizing dosing and timing parameters using flank allografts, female athymic nude mice bearing flank xenografts ($n = 3$ per cell line) were intravenously administered VGT-309 at a dose of 2 mg/kg. As a negative control, mice bearing KB flank xenografts were administered 50 mg/kg JPM-OEt via intraperitoneal injection daily for 5 days prior to VGT-309 administration. As a positive control, mice bearing KB flank xenografts were administered the JPM-OEt delivery vehicle without the cathepsin inhibitor via intraperitoneal injection daily for 5 days prior to VGT-309 administration. Twenty-four hours after VGT-309 injection, mice were euthanized and imaged with the Iridium Imaging System (Vision Sense, New York, NY). Tumors were removed and imaged with the Odyssey Imaging System (LI-COR Biosciences, Lincoln, NE). Tissue sections were further analyzed by hematoxylin and eosin (H&E) staining, as well as fluorescence microscopy (Leica Microsystems, Wetzlar, Germany).

Flow cytometric analysis of probe-labeled cells in small animal models

Female athymic nude mice harboring GFP-transfected human pulmonary adenocarcinoma (A549-GFP) flank xenografts were injected with either VGT-309 (2 mg/kg) or PBS vehicle, and tumors were collected 24 hours after injection. Harvested tumors were minced and digested in Liberase TL (Roche, ref# 5401020001) for 30 minutes at 37°C. After quenching with FBS, tumor fragments were passed through 100-μm nylon cell strainers, washed in PBS with 1% FBS, and passed through a 40-μm strainer. After processing into cell suspensions, all samples were immediately analyzed by flow cytometry.

Total cells dissociated from tumors were incubated with anti-mouse CD16/32 BV785 conjugated anti-mouse CD45 IgG, phycoerythrin-conjugated anti-mouse CD11b IgG, and phycoerythrin-

Cy5 conjugated anti-mouse F4/80 IgG, (all from BioLegend, San Diego, CA). Data were collected from at least 200,000 cells by LSRFortessa (BD Biosciences, Franklin Lakes, NJ) and analyzed by FlowJo (Tree Star Inc., Ashland, OR).

Dose-escalation study of IMI with VGT-309 in canines undergoing pulmonary resection

A pilot study of IMI with VGT-309 was approved by the University of Pennsylvania IACUC and the School of Veterinary Medicine Animal Protocol Committee. The owners of all subjects ($n = 4$) provided written informed consent. Subjects had previously undergone chest X-rays that were reviewed by a specialized thoracic radiologist to confirm the presence of a pulmonary tumor and identify other suspicious nodules.

On the day of pulmonary resection, study participants received either 0.1 mg/kg or 0.3 mg/kg intravenous VGT-309 3 hours prior to resection. One subject received the tracer 18 hours prior to resection. A starting dose of 0.3 mg/kg (6 mg/m^2) VGT-309 was chosen on the basis of the estimated effective dose of 2 mg/kg in mice, which often corresponds to a lower effective dose in canines owing to differences in the ratio of body surface area to body weight (23, 24). The dose was reduced to 0.1 mg/kg (2 mg/m^2) after two dogs receiving 0.3 mg/kg showed strong tumor fluorescence. The goal of the second dose cohort was to determine if whether a lower dose of VGT-309 would also provide strong tumor contrast. During pulmonary resection, surgeons used visual inspection and finger palpation through a thoracotomy incision to confirm the lesion in the lobe of interest. Nodules were then imaged using the Iridium NIR imaging system (Vision Sense, New York, NY). The Iridium is a high definition, dual band (white light and NIR) camera system capable of NIR emission and detection. A 805-nm excitation source was used, and fluorescence was detected using a bandpass filter ranging from 825 nm to 850 nm. For thoracoscopic resections, the Iridium was equipped with a 5-mm, 0-degree thoracoscope. The integration time of the imaging system is 45 milliseconds. For *ex vivo* evaluation, a free-standing exoscope was used. The field of view is approximately 19 × 14 cm with a working distance of 40 cm. The system is capable of variable gain but gain was fixed at 50% for standardization across subjects. TBRs were calculated by comparing the fluorescence intensity overlying areas of clinically apparent tumor and compared with the fluorescence intensity of regions of normal appearing lung. TBR calculations were repeated in triplicate and averaged. Minimum ROI size was at least 1,000 pixels. All specimens underwent pathologic examination by a board certified veterinary pathologist. In addition, resected specimens were evaluated using a NIR microscopic scanner (Odyssey, LI-COR Biosciences) to assess patterns of VGT-309 accumulation.

Phase I study of VGT-309 in healthy human volunteers

A Phase I randomized, double-blind, placebo-controlled, single ascending dose study in healthy subjects was performed to evaluate the safety, tolerability, and pharmacokinetics of VGT-309 without the overlying effects of controlled surgical trauma. The study was registered with the Australian New Zealand Clinical Trials Registry (anzctr.org.au; registration number ACTRN12620000948998), approved by the Alfred Human Research Ethics Committee, and performed at the Centre for Clinical Studies, Nucleus Network, Melbourne, Victoria, Australia. The study was conducted in full compliance with Good Clinical Practice and Therapeutic Goods Administration guidelines. All patients provided written informed consent and studies were conducted in accordance with the Declaration of Helsinki guidelines.

The initial study dose of 0.016 mg/kg (0.6 mg/m^2; Cohort 1) was selected on the basis of a 100-fold safety margin applied to the 3 mg/kg (60 mg/m^2) no-observed-effect level (NOEL) in dogs determined in a single-dose toxicity study conducted in compliance with Good Laboratory Practices (GLP) at ITR Laboratories (Montreal, Quebec, Canada). The subsequent prespecified dose levels were 0.05 mg/kg (2 mg/m^2, Cohort 2), 0.16 mg/kg (6 mg/m^2, Cohort 3), and 0.32 mg/kg (12 mg/m^2, Cohort 4), covering the estimated effective dose found in mice of 2 mg/kg (human equivalent dose = 0.16 mg/kg) based on standard allometric scaling.

Following patient informed consent and eligibility screening, a total of 30 subjects were enrolled and randomized to receive VGT-309 or placebo (normal saline) in 1 of 4 dose cohorts as follows: 8 at 0.016 mg/kg (6 VGT-309, 2 placebo); 8 at 0.050 mg/kg (6 VGT-309, 2 placebo); 7 at 0.16 mg/kg (5 VGT-309, 2 placebo); and 7 at 0.32 mg/kg (6 VGT-309, 1 placebo). Each subject had baseline safety assessments consisting of a physical exam, vital signs, chemistry, hematology, coagulation and urinalysis clinical laboratory studies, and electrocardiogram (ECG) prior to receiving a single intravenous infusion of VGT-309 or placebo over 15 to 20 minutes. Safety assessments (physical exam, vital signs, clinical laboratory studies, ECG, solicitation of adverse events) were taken during the first 24 hours after dosing, a week after dosing, and 30 days after dosing. Solicitation of adverse events also occurred 48 hours after dosing. Blood samples for pharmacokinetic analysis were drawn prior to dosing and 10, 30, and 45 minutes and 1, 2, 3, 4, 6, 8, 12, 18, 24, and 48 hours after dosing. The bioanalytical assay for VGT-309 levels in human plasma was performed by 360biolabs (Melbourne, Australia). Dose escalation for each cohort occurred once the previous dose was deemed to be safe and well tolerated following review of safety data up to Day 7 by the Safety Review Committee.

Adverse events were defined in accordance with the FDA Safety Guidance, referencing 21CFR312.32 (a), as any untoward medical occurrence associated with the use of a drug in humans, whether or not considered drug related. Adverse event relationship to investigational product was determined by the Principal Investigator and assessed using the definitions that follow. An adverse event was considered related if there was a distinct temporal relationship between the event onset and administration of the investigational agent, there was a known reaction to agent or chemical group or predicted by known pharmacology, and/or the event could not be explained by a subject's clinical state or other factors. An adverse event was considered unrelated if evidence existed that the event had an etiology other than the investigational product, such as preexisting condition, underlying disease, intercurrent illness, or concomitant medication.

Study of IMI with VGT-309 in humans undergoing pulmonary resection

As part of an ongoing, open label, Phase II human study, patients with lung lesions suspicious for malignancy were enrolled beginning in May 2021. The study was registered with the Australian New Zealand Clinical Trials Registry (anzctr.org.au; registration number ACTRN12621000301864), approved by the St. Vincent's Hospital, Melbourne Human Research Ethics Committee, and was performed at St. Vincent's Hospital, Melbourne, Australia. All subjects provided written informed consent. VGT-309 was intravenously administered on the day prior to resection at one of two doses (0.16 or 0.32 mg/kg). During minimally invasive video-assisted thoracic surgery, surgeons first used thoracoscopic visualization and finger palpation to identify known lesions. Next, the surgical field was imaged with a standard clinical grade optical imaging device (Stryker 1588 Advanced Imaging

Modality Platform, Stryker Corporation, Kalamazoo, MI) with an external light source providing both white light for visible light imaging and 805-nm laser illumination for optimal excitation of ICG fluorescence. Fluorescence was assessed in the primary lesion *in situ* and the resection specimens were also imaged *ex vivo* before being sent for pathologic analysis. In this trial, surgeons adhered to standard-of-care principles of oncologic resection as guided by frozen section pathology. There were no alterations in resection margins based solely upon fluorescence imaging, given that the efficacy of this technology has not yet been confirmed.

Histopathologic and fluorescent microscopic review of specimens

As described previously (25), specimens were formalin fixed and paraffin embedded. Sequential 5-μmol/L sections were obtained and underwent comprehensive histopathologic and fluorescent analysis by a board-certified thoracic pathologist. Sections were stained using standard H&E staining. IHC staining for CD45 was also performed. To understand VGT-309 accumulation patterns at a microscopic level, an additional unstained 5-μm section was evaluated using a NIR microscopic scanner (Odyssey, LiCor, Lincoln, NE) and a NIR microscope (Leica Microsystems, Buffalo Grove, IL). Areas of fluorescence were then correlated to both H&E and anti-CD45 IHC specimens.

Post hoc image analysis

Post hoc image analysis was conducted with ImageJ (http://rsb.info.nih.gov/ij). Mean fluorescence intensity (MFI) of the lesion (MFI_{lesion}) was obtained by analyzing monochromatic NIR images and measuring the ROI, which correlated to the lesion. Background fluorescence (0.5–1.0 cm from margin) was also obtained ($MFI_{background}$). Calculations were repeated in triplicate, and signal-to-background fluorescence ratios (SBR) were calculated using the following equation ($MFI_{lesion}/MFI_{background}$). SBR assessments were averaged, and a mean SBR > 2.0 was considered fluorescent.

Statistics

For *in vitro* assays and *in vivo* murine studies, at least 3 samples were used per group unless noted. *Post hoc* image analysis was performed to quantify the amount of fluorescence using ROI software within ImageJ (NIH; https://imagej.nih.gov/ij) as described previously (26). A background fluorescence level was similarly obtained, and target- or tumor-to-background (TBR) was calculated. For preclinical (*in vitro* and animal data), results are expressed as mean (SD) unless otherwise noted. All comparisons were made using Stata Statistical Software release 14 (StataCorp, College Station, TX). Student *t* tests were used for statistical comparison unless otherwise noted. A *P* value of 0.05 or less was considered statistically significant.

Data availability

The data in this study are available upon reasonable request to the corresponding author.

Results

Human lung cancer cells express cathepsins that are fluorescently labeled by VGT-309

To study the ability of VGT-309 to label human lung cancer at the cellular level, we first performed Western blot analysis to confirm cathepsin expression in four human NSCLC cell lines of varying histopathologic subtypes (**Fig. 1B**). These included A549 (adenocarcinoma), H460 (large cell carcinoma), H513 (adenosquamous cell carcinoma), and H1264 (squamous cell carcinoma). We chose the human cervical carcinoma cell line KB as a positive control in our experiments, given its previous use as a control in studies of cathepsin expression in human tumors (18). To evaluate the binding specificity of VGT-309 to individual cysteine cathepsins as well as the activity dependence of the probe, we incubated A549 cells with 1 μmol/L VGT-309 for 2 hours after pretreatment of cells for 30 minutes with 100 μmol/L JPM-OEt, a pan-cathepsin inhibitor. This inhibitor binds irreversibly in the active site of the cysteine cathepsins, thus blocking the binding of VGT-309. We collected and lysed these cells and analyzed the lysates by SDS-PAGE to resolve individual cathepsins by molecular weight. We found that VGT-309 labeled cathepsins B, L, S, and X. Furthermore, pretreatment with JPM-OEt blocked labeling of all cathepsins, confirming the high degree of selectivity of the probe (**Fig. 1C**).

To assess the localization and internalization of VGT-309, we imaged live A549 cells at various time points after staining with 1 μmol/L VGT-309 and 200 nmol/L Lyso-Tracker. We found that VGT-309 freely entered cells and covalently modified active cysteine cathepsins resulting in unquenching of the probe. Fluorescent signal was primarily lysosomal in distribution (**Fig. 1D**). To assess dosing, we incubated A549 cells with increasing concentrations of VGT-309 and imaged cells by fluorescence microscopy after 2 hours of probe labeling. There was a clear dose-dependent relationship between concentration of VGT-309 and fluorescence at the cellular level, with near total elimination of signal in cells pretreated with JPM-OEt (**Fig. 1E** and **F**).

VGT-309 fluorescently labels pulmonary tumors in xenograft mouse models

To evaluate the biodistribution, optimal dosing, and time to imaging of VGT-309, we randomized female athymic nude mice bearing flank KB xenografts measuring 250 ± 50 mm^3 to intravenous VGT-309 delivery at 3 dosage levels: 1.0 mg/kg (3 mg/m^2), 2.0 mg/kg (6 mg/m^2), and 4.0 mg/kg (12 mg/m^2; $n = 5$ per dosing level). After tail vein injection, we recorded the fluorescence of tumor and background tissue (contralateral flank) at several time points using the Iridium *In Vivo* Imaging System (**Fig. 2A**). The tumor margin could be delineated by fluorescent signal as soon as 15 minutes after injection of 2 mg/kg VGT-309. *In vivo* tumor fluorescent signals continued to increase up to 24 hours after VGT-309 injection (**Fig. 2B**) with peak mean SBR of 3.12 for the 2 mg/kg group and 2.26 for the 4 mg/kg group (**Fig. 2C**). *Ex vivo* organ biodistribution analysis at 24 hours showed that tumors displayed strong fluorescent signal (mean MFI: 58.89 A.U.) with fluorescent signal in the kidneys, liver, and spleen consistent with known cathepsin expression in these tissues (**Fig. 2D** and **E**; refs. 18, 27, 28). On the basis of these biodistribution and time course data, the optimal imaging dose was determined to be 2 mg/kg and optimal imaging time was 24 hours after injection.

To determine if VGT-309 could label human pulmonary tumor xenografts, female athymic nude mice bearing A549 (human adenocarcinoma), H460 (human large cell carcinoma), H513 (human adenosquamous cell carcinoma), and H1264 (human squamous cell carcinoma) flank xenografts ($n = 3$ per group) were administered 2 mg/kg VGT-309 via tail vein injection. Mice bearing KB (human cervical carcinoma) xenografts were used as a positive control, and those bearing KB xenografts pretreated with 50 mg/kg JPM-OEt via intraperitoneal injection daily for 5 days prior to VGT-309 administration were used as a negative control. Twenty-four hours after VGT-309 injection, mice were sacrificed and imaged with the Iridium NIR imaging system.

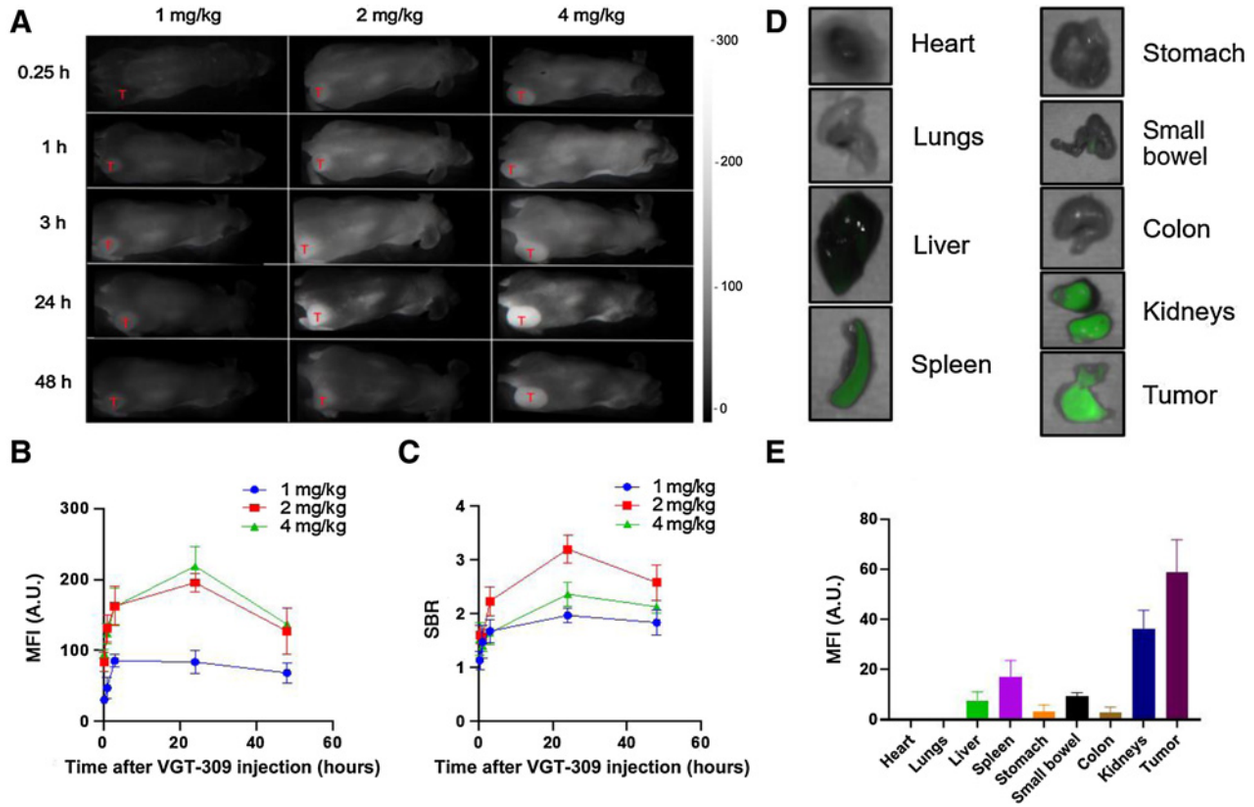

Figure 2.

Dosing, timing, and biodistribution of VGT-309 in mice. **A,** Mice bearing KB flank xenografts were administered VGT-309 at increasing dosing levels then imaged with the Iridium NIR Imaging System. Representative NIR images of mice are shown at various times after intravenous drug delivery with red "T" marking location of the flank xenograft in each mouse. **B,** MFI of flank tumors over time and at various VGT-309 doses. Points represent mean values with SD. **C,** SBRs were obtained for each dosing level and plotted over time from drug delivery. Each point represents an individual mouse. **D,** Twenty-four hours after delivery of VGT-309 at 2 mg/kg, mice were euthanized to determine drug biodistribution via fluorescence of organs and tumors. **E,** Bar graph demonstrating fluorescence of flank tumors as compared with other organs. Bars indicate means with SD.

Xenografts derived from all four human lung cancer cell lines displayed strong macroscopic fluorescent signal (**Fig. 3A**). Pretreatment of xenograft-bearing mice with a pan-cathepsin inhibitor nearly eliminated fluorescent signal from flank tumors, indicating cathepsin-activity dependence of the fluorescent signal. On *post hoc* analysis of fluorescent images, the ROI corresponding to flank tumors had significantly higher MFI than those corresponding to background tissue on the contralateral flank of the same mice (**Fig. 3B**; $P < 0.0001$ in all cases). There were no significant differences between MFI for tumor and background tissue in the mice pretreated with pan-cathepsin inhibitor. Mean SBR was greater than 2.0 for all lung cancer xenografts, indicating excellent tumor-specific labeling (**Fig. 3C**; ref. 29). Microscopic analysis of tumor sections confirmed cathepsin activity–dependence of VGT-309 labeling, as fluorescent signal was absent on sections of tumors harvested from mice pretreated with JPM-OEt (**Fig. 3D**).

VGT-309 labels tumor cells and TAMs in mice

Because tumors consist of cancer and stromal cells, which also express cathepsins, we next investigated to what extent VGT-309 labeled tumor cells as compared with TAMs using mice bearing A549 flank xenografts that express GFP. After 24 hours, tumors resected from mice injected with VGT-309 had a significantly higher proportion of ICG+ fluorescent cells compared with control animals given saline (**Fig. 4A** and **D**; 12.9% vs. 0.4%; $P = 0.010$). The majority of VGT-309–labeled cells were GFP+ tumor cells, and a smaller population were CD45+ leukocytes (**Fig. 4B** and **E**; 77.6% vs. 19.6%; $P = 0.006$). Of the CD45+ cells labeled by VGT-309, greater than 80% were CD11b+/F4/80+ TAMs (**Fig. 4F**). Analysis of the non–VGT-309 labeled cell population confirmed that VGT-309 labeling was selective for tumor cells and TAMs (Supplementary Fig. S1 for representative case). Fluorescence microscopy of resected tumors confirmed that the majority of VGT-309–labeled cells were GFP-expressing cancer cells (**Fig. 4G**).

VGT-309 accumulates in spontaneously occurring canine tumors

For the purposes of evaluating clinical feasibility, we conducted a canine study of VGT-309 during pulmonary tumor resection. Four companion animals with spontaneous lung tumors were enrolled in the study. Ages ranged from 6 to 10 years (mean 7.75 years) and weights ranged from 14.6 to 30.3 kg (mean 21.1 kg). The VGT-309 infusions were well tolerated and no adverse reactions were observed. Two dogs had pulmonary adenocarcinomas, one had a minimally invasive pulmonary adenocarcinoma, and one had a pulmonary

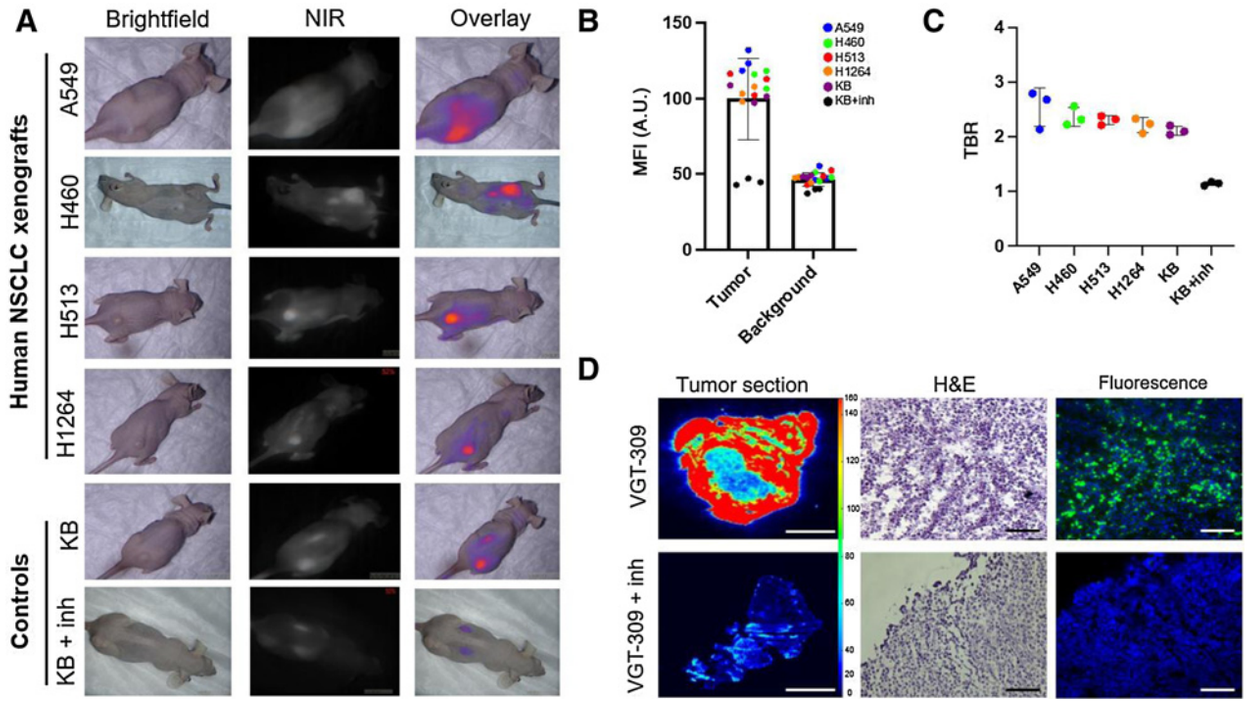

Figure 3.

VGT-309 labels human NSCLC xenografts. **A,** Representative brightfield, NIR, and overlay images of mice bearing various NSCLC flank xenografts ($n = 3$/cell line) 24 hours after injection of 2 mg/kg VGT-309. Mice bearing KB flank xenografts ($n = 3$) pretreated with 50 mg/kg JPM-OEt via intraperitoneal injection for 5 days before VGT-309 administration served as a negative control and those pretreated with delivery vehicle ($n = 3$) served as a positive control. **B,** MFI of tumor and background tissue with symbol color indicating cell line. **C,** SBRs from the flank xenografts. Each point represents a single tumor with means and error bars displayed for each group. **D,** Correlative *ex vivo* histopathology and fluorescence microscopy of flank xenografts from mice without (top) and with JPM-OEt pretreatment (bottom). The leftmost column depicts heatmaps of macroscopic tumor fluorescence. The center column shows H&E-stained tissue slides. The rightmost column shows fluorescence microscopy. Green signal represents VGT-309 and blue signal shows DAPI staining. VGT-309 signal is absent in mice pretreated with a cathepsin inhibitor, demonstrating the cathepsin-activity dependence of VGT-309 fluorescence. Scale bars represent 50 μm.

carcinoma. Mean tumor size was 2.9 cm (range, 2.5–3.5 cm). Canine characteristics are summarized in **Table 1**.

On the day of pulmonary resection, study participants received either 0.1 mg/kg (2 mg/m^2) or 0.3 mg/kg (6 mg/m^2) intravenous VGT-309 three hours prior to resection. One subject received the tracer 18 hours prior to resection. A starting dose of 0.3 mg/kg (6 mg/m^2) VGT-309 was chosen on the basis of the estimated effective dose of 2 mg/kg (6 mg/m^2) in mice, which often corresponds to a lower effective dose in canines owing to differences in the ratio of body surface area to body weight (23, 24). Timing of VGT-309 dosing in canines differed from that used in murine and human studies due to logistical issues that prevented most canine owners from making two separate trips to the veterinary hospital (i.e., on the day prior to surgery for VGT-309 infusion and on the day of surgery).

All four dogs underwent thoracotomy for tumor resection and tumors were imaged *in situ* with the Iridium NIR Imaging System (**Fig. 5A**). All tumors displayed a high degree of fluorescence with mean tumor MFI of 144.97 A.U. as compared with background MFI of 55.34 A.U. (**Figure 5B**; $P < 0.0001$). SBRs ranged from 2.15 to 3.71 (**Fig. 5C**). There were no significant differences in fluorescence when comparing the 0.1 mg/kg and 0.3 mg/kg dosing groups.

Following tumor resection, each specimen was reimaged on the back table using the NIR imaging device. Tumors displayed robust *ex vivo* fluorescence with mean tumor MFI of 141.75 A.U. as compared with background MFI of 53.76 A.U. ($P < 0.0001$). SBRs ranged from 2.03 to 2.64. A stitch was placed using fluorescence guidance at the macroscopic tumor border and in the normal lung in all radial directions prior to submission to pathology. Pathology analysis confirmed tumor presence at the areas of fluorescence and normal lung at the location of background fluorescence (**Fig. 5D** and **E**; Supplementary Fig. S2).

VGT-309 is safe in humans

To evaluate the safety profile of VGT-309 without the overlying effects of controlled surgical trauma and to assure an understanding of the pharmacokinetic profile before starting an imaging study, a single ascending dose study was performed in healthy volunteers. In this study, a single intravenous infusion of VGT-309 or placebo (normal saline) was administered to 4 sequential cohorts of 7 to 8 subjects for a total of 30 subjects, 23 receiving VGT-309 and 7 receiving placebo. The initial study dose of 0.016 mg/kg (0.6 mg/m^2; Cohort 1) was selected on the basis of a 100-fold safety margin applied to the 3 mg/kg (60 mg/m^2) NOEL in dogs determined in a single-dose toxicity study conducted in compliance with GLP at ITR Laboratories (Montreal, Quebec, Canada). The subsequent prespecified dose levels were 0.05 mg/kg (2 mg/m^2, Cohort 2), 0.16 mg/kg (6 mg/m^2, Cohort 3), and 0.32 mg/kg (12 mg/m^2, Cohort 4), covering the estimated effective dose found in mice of 2 mg/kg (human equivalent dose = 0.16 mg/kg) based on standard allometric scaling. VGT-309 was well tolerated in all four doses studied with neither an observed trend in treatment-emergent

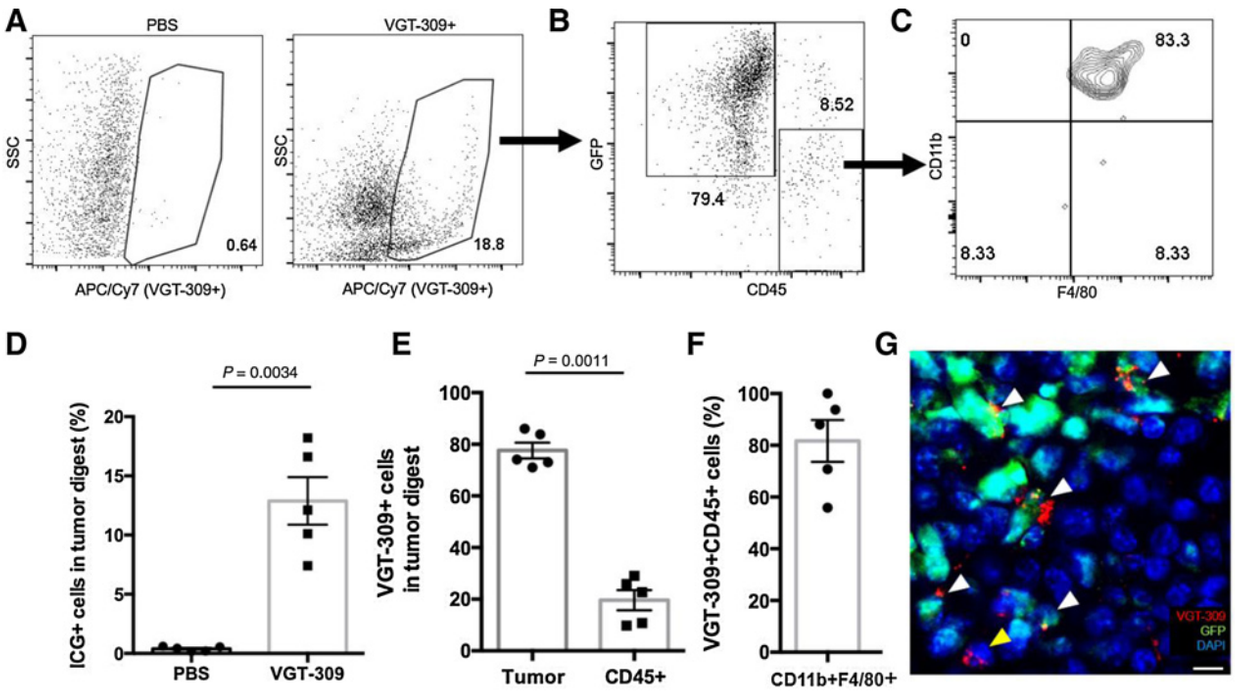

Figure 4.

VGT-309 labels tumor cells in a murine flank xenograft model of NSCLC. **A,** Representative flow cytometric analysis of resected A549 flank xenograft tumors expressing tumor cell–specific GFP after intravenous administration of PBS or VGT-309 (2 mg/kg). $Cy7^+$ cells (outlined, cells with fluorescence $>3 \times 10^5$) were sorted and quantified ($n_{PBS} = 4$ mice, $n_{VGT\text{-}309} = 4$ mice). **B,** In the $Cy7^+$ cells, the proportions of GFP^+ tumor cells and $CD45^+$ leukocytes were further quantified ($n = 4$ mice). **C,** In the CD45+ cells, the proportion of CD11b+F4/80+ cells (TAMs) were further quantified. **D,** Bar graphs indicating the percent of ICG+ cells in tumors treated with VGT-309 or PBS vehicle. **E,** Bar graphs indicating the percent of dye-labeled cells that were GFP+ tumor cells or CD45+ leukocytes. **F,** Bar graph showing the percent of CD45+ leukocytes that were CD11b+F4/80+ TAMs. *P* values were determined by unpaired *t* test. **G,** Fluorescence microscopy of a resected A549-GFP flank xenograft at 40x magnification. Channels at VGT-309 (red), GFP (green), and DAPI (blue) emission wavelengths are overlaid, showing that the majority of VGT-309 labeled cells are GFP-expressing cancer cells (white arrowheads) with minimal labeling of non-GFP expressing stromal cells (yellow arrowhead). Scale bar represents 10 μm.

adverse events (TEAE) nor any observed serious adverse events (**Table 2**). A total of 15 TEAEs were recorded in 9 subjects (2 in the placebo group, and 13 in the VGT-309 cohorts). All TEAEs were deemed mild to moderate in severity (15 mild, 2 moderate). In subjects given VGT-309, 9 of the TEAEs were deemed unrelated and 4 deemed related (2 in Cohort 2 and 2 in Cohort 4).

The 4 drug-related TEAEs occurred in 2 subjects. One subject in Cohort 2 (0.05 mg/kg) reported mild nausea and lightheadedness. The other subject (0.32 mg/kg; Cohort 4) had a moderate reaction beginning 2 minutes after initiation of infusion, which consisted of chest heaviness, nausea, dizziness, and transient mild hypotension and tachycardia. The dose was immediately interrupted and the infusion reaction rapidly subsided. Blood samples taken immediately after the event showed no increase in tryptase or complement levels, indicating the infusion reaction was not due to an IgE mast cell–mediated process or complement activation. While the cause of the infusion reaction remains unclear, there were no laboratory findings to suggest an allergic etiology.

Pharmacokinetic characterization of Cohorts 1 and 2 was incomplete due to VGT-309 plasma levels falling rapidly below the VGT-309 bioanalytical sensitivity limits after infusion, while Cohorts 3 and 4 provided accurate data out to 24 hours and 48 hours, respectively. The pharmacokinetic profiles for subjects in Cohorts 3 and 4 showed an initial rapid decline in VGT-309 concentrations

Table 1. Clinical and demographic characteristics of canines undergoing VGT-309–guided pulmonary resection.

Patient number	Sex	Age (years)	Breed	Weight (kg)	Tumor size (cm)	Tumor location	Final diagnosis	VGT-309 dose	Hours from infusion to surgery
1	M	6	Labrador mix	23.9	2.5	R caudal lung lobe	Pulmonary carcinoma	0.1 mg/kg	3
2	F	7	Boxer	30.3	2.5	R caudal lung lobe	Pulmonary adenocarcinoma	0.1 mg/kg	3
3	M	10	Beagle	14.6	3.5	R caudal lung lobe	Pulmonary adenocarcinoma	0.3 mg/kg	3
4	F	8	Beagle	15.5	2.9	R caudal lung lobe	Minimally invasive pulmonary adenocarcinoma	0.3 mg/kg	18

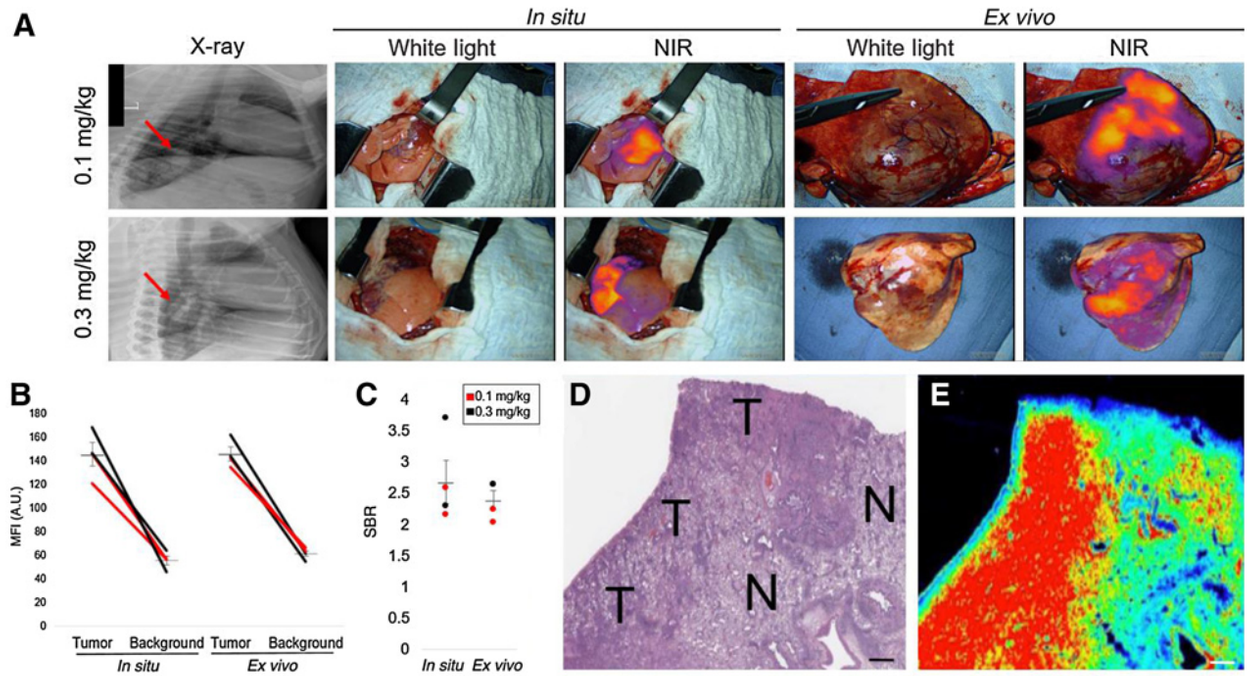

Figure 5.

VGT-309 labels spontaneously occurring pulmonary tumors in canines. **A,** Representative preoperative and intraoperative images from canines preoperatively infused with 0.1 mg/kg or 0.3 mg/kg VGT-309. Tumors were clearly identifiable by NIR imaging both *in situ* and *ex vivo* after resection. **B,** MFI of tumor and background tissue *in situ* and *ex vivo*. Lines represent paired tumor and background measurements from the same patient. Lines are colored according to VGT-309 dose. Mean bars with SD are shown. **C,** SBR of all tumors in the study, both *in situ* and *ex vivo*. Each point represents an individual tumor with mean bars with SD also shown. Points are colored according to the VGT-309 dose. **D** and **E,** Correlative histopathology and fluorescence imaging, respectively, of a representative resected tumor. T denotes areas of tumor with N marking normal canine lung. Fluorescence intensity of VGT-309 labeling is spatially concordant with tumor. Scale bars represent 100 μm.

post-infusion, followed by a terminal phase with half-lives of 7.8 and 9.5 hours, respectively. Individual subject half-lives for Cohort 4, the cohort with the greatest degree of pharmacokinetic characterization, ranged from 7.9 hours to 13.6 hours (Supplementary Fig. S3). Analysis of the Phase I safety and pharmacokinetic data indicate that VGT-309 is well tolerated and safe to use at all four doses studied.

VGT-309 selectively labels non-palpable human lung cancers during resection

A Phase II trial of VGT-309 for guidance of lung cancer resection is currently in progress. Because all four doses in the Phase I single ascending dose study in healthy human volunteers were deemed safe, we started the Phase II trial with an initial dose of 0.05 mg/kg (2 mg/m^2) based on the efficacious dose of 0.1 mg/kg (2 mg/m^2) observed in companion dogs. The dose was sequentially increased to 0.16 (6 mg/m^2) and 0.32 mg/kg (12 mg/m^2) to determine the optimal dose for both efficacy and safety. The full results of the trial will be reported in a separate manuscript, but two representative patients are presented here to illustrate (i) the successful clinical translation of this novel tracer and (ii) its potential to improve surgical management of patients undergoing cancer resection.

Patient 1006 is a 57-year-old male who presented with a 45-mm PET-avid right lung mass without evidence of extrapulmonary disease. He was infused with 0.16 mg/kg (6 mg/m^2) VGT-309 on the day prior to surgery. Intraoperatively, his primary tumor was visible, palpable, and showed robust *in situ* fluorescence when imaged with an NIR thoracoscope (**Fig. 6A**; SBR, 7.18). Final histopathologic analysis confirmed adenocarcinoma with microscopic concordance between tumor cells and VGT-309 fluorescence.

Patient 1011 is a 68-year-old female with a history of contralateral lung cancer (previously resected by lobectomy) who presented with a 17-mm PET-avid left lung nodule suspicious for malignancy. Given concern for a metastasis from the previous lung cancer, the planned operation was a sublobar wedge resection with appropriate margins. She was infused with 0.32 mg/kg (12 mg/m^2) VGT-309 on the day prior to surgery. Intraoperatively, the surgeon was unable to locate the primary tumor using white light and digital palpation alone. Without fluorescence imaging, the surgeon would have converted to an open thoracotomy to locate and remove the tumor. However, upon inspection with the Stryker 1588 NIR imaging system, the VGT-309–labeled tumor was immediately identified (**Fig. 6B**; SBR, 2.83), allowing the surgeon to confidently remove the tumor by wedge resection and spare normal lung parenchyma in this patient with baseline compromised pulmonary function. Microscopic fluorescence was spatially concordant with tumor cells and final histopathologic diagnosis was adenocarcinoma (**Fig. 6C**). Resection margins were clear of tumor by histopathology, and genomic testing by next-generation sequencing of the tumor confirmed that this was a solitary metastasis from the previous lung cancer. A CT scan 3 months postoperatively confirmed complete resection of the nodule without evidence of recurrence.

Table 2. TEAEs in a Phase I dose-ascending study of VGT-309 in healthy volunteers.

Subject ID	Dose (mg/kg)	Age	Sex	Weight	TEAEs		
					Adverse event	Severity	VGT-309 relatedness
1009	0.016	32	M	86.5			
1011	0.016	18	M	90.2	Pain at IVC site	Mild	Unrelated
1017	0.016	21	M	82.3			
1019	0.016	19	F	67.8	Headache	Mild	Unrelated
1020	0.016	22	M	65			
1021	0.016	29	F	79.9			
1006	0.05	25	M	69.7			
1018	0.05	22	M	59.5	Nausea	Mild	Related
					Lightheadedness	Mild	Related
1031	0.05	26	M	92.4			
1032	0.05	22	F	67.9	Menstrual cramps	Mild	Unrelated
1036	0.05	42	M	83.6			
1040	0.05	19	F	58.7			
1045	0.16	37	F	73.1			
1049	0.16	33	M	80.6			
1051	0.16	21	F	66.5			
1056	0.16	27	M	79.3			
1059	0.16	22	M	70.9			
1063	0.32	25	M	61.3	Postural dizziness	Mild	Unrelated
1070	0.32	51	F	83.5	Nausea	Mild	Unrelated
					Headache	Moderate	Unrelated
1071	0.32	19	F	63.7	Nausea	Mild	Unrelated
					Lower back pain	Mild	Unrelated
1073	0.32	27	F	63.3			
1079	0.32	18	M	72.5	Loose bowel movement	Mild	Related
					Infusion-related reaction	Moderate	Related
					Chest pain	Mild	Unrelated
1084	0.32	23	F	69.9			
1013	Placebo	31	F	51.4			
1024	Placebo	26	F	53.2			
1010	Placebo	22	M	79			
1035	Placebo	29	F	53			
1042	Placebo	26	M	84.4	Right IVC site bruise	Mild	Unrelated
					Left cubital fossa bruising	Mild	Unrelated
1060	Placebo	25	F	55			
1072	Placebo	40	M	92.7			

Discussion

In this study, we evaluated a cathepsin-targeted, quenched activity–based NIR probe for identifying tumors during resection. Using multiple small and large animal models, we demonstrated that VGT-309 reliably labels a broad range of NSCLCs during resection. Finally, we report preliminary evidence from a pilot human study to demonstrate the successful translation of the probe to patients undergoing cancer resection, as well as the clinically meaningful impact it may have in identifying visually occult tumors in real time. To our knowledge, this is the first study to test a covalent activity–based NIR probe during resection of human tumors.

This work builds upon a robust body of preclinical literature evaluating the utility of cathepsin-targeted probes for imaging cancer. This has included many studies in cellular systems and animal models of cancer (10, 11, 16, 17, 30–32). More recently, a cathepsin substrate probe containing a far-red fluorophore, LUM015, was used to image human breast and sarcoma resection specimens (33). Smith and colleagues evaluated the same probe in *ex vivo* breast cancer resection specimens and have also demonstrated its ability to detect residual cancer when resection cavities were imaged (34, 35). Because LUM015 requires a tracer-specific imaging device to detect signal in the far-red spectrum, its depth of penetration is limited to surface level tumors and its clinical adoption may be hindered by the fact that the imaging device for its detection is not widely available.

To improve depth of tumor detection and allow compatibility with existing, FDA-approved clinical imaging devices, recent work has focused on designing cathepsin-targeted probes in the NIR spectrum (32, 36, 37). In a large review of IMI-guided lung cancer resections, NIR probes were shown to have a depth of penetration of 1.7 cm below the pleural surface (38). Not only do NIR probes generate deeper depth of signal penetration, they can also be detected by commercially available surgical imaging devices used to detect ICG. Several groups have developed and tested cathepsin-targeted probes in the NIR range and have shown tumor-specific labeling in preclinical studies of breast, colorectal, and skin cancer (8, 31, 30). The FDA has recently approved a folate receptor–targeted NIR contrast agent, pafolacianine, which has shown efficacy in clinical trials of image-guided resection of ovarian and lung cancer (39–42). However, this probe is limited by the fact that it is not a "smart" probe and can only detect tumors that overexpress folate receptor.

Here, we show that VGT-309 selectively labels a wide range of NSCLCs during surgical resection. Flow cytometric studies of tumors

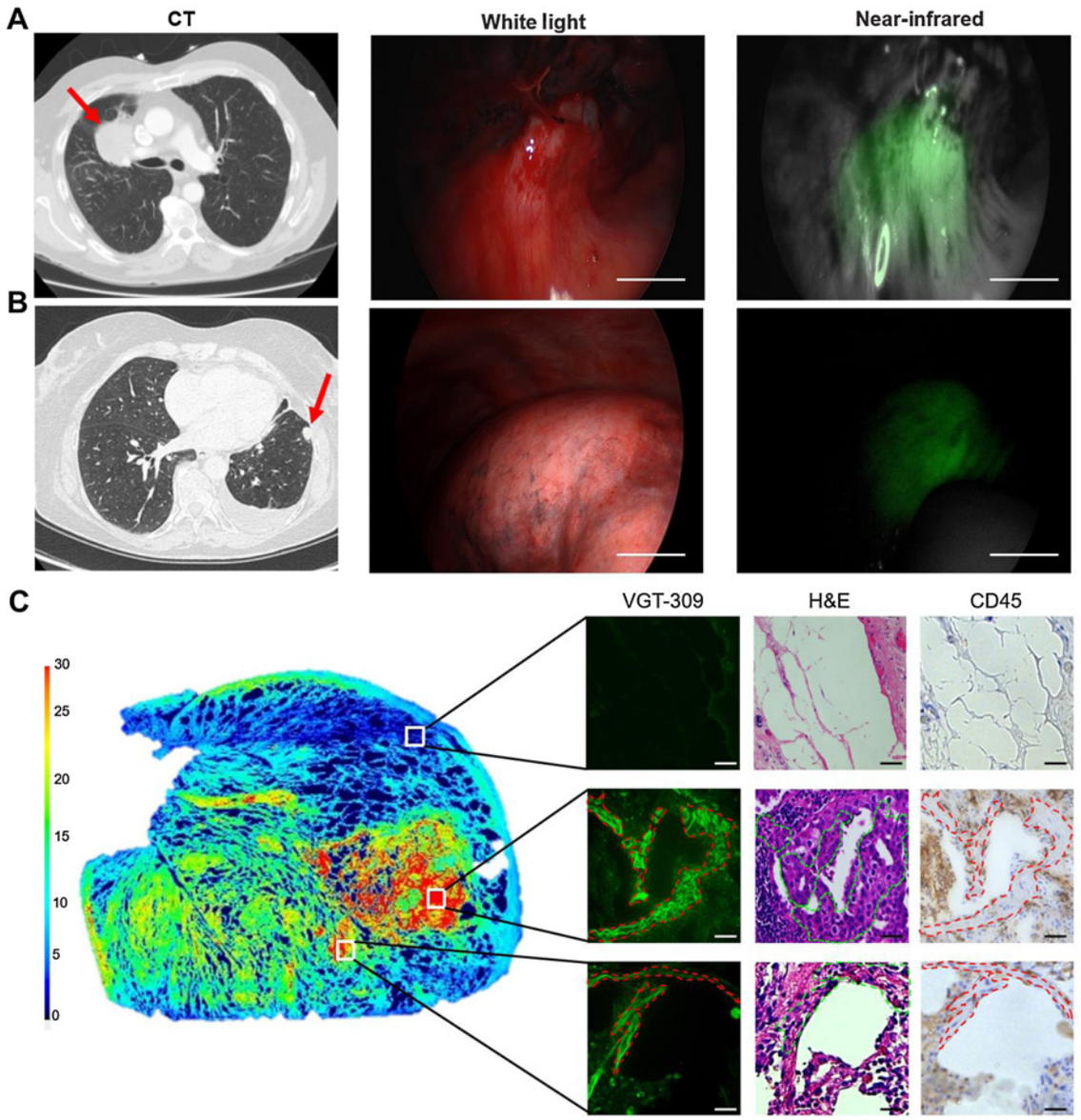

Figure 6.

VGT-309 labels human pulmonary tumors during resection. **A** and **B,** Representative preoperative and intraoperative images of palpable and non-palpable pulmonary tumors, respectively. Red arrows label tumor locations in preoperative CT imaging. VGT-309 clearly identified both tumors *in situ* with SBR ratio of greater than 2.0 in both cases. Scale bars represent 1 cm. **C,** On microscopic analysis of tissue sections, VGT-309 fluorescence was spatially concordant with malignant cells by histopathology and IHC with limited immune cell (CD45+) labeling. Fluorescence imaging of an entire 5-μm tissue section is shown at left with white boxes indicating the areas of magnification. Paired fluorescence microscopy, H&E staining, and IHC for CD45 are shown at right under 20x magnification. Images were reviewed by a board-certified thoracic pathologist with specific determinations of malignancy as noted by dashed lines. Scale bars represent 50 μm.

from VGT-309–injected mice showed that most fluorescently labeled cells were tumor cells, but a significant portion of labeled cells were TAMs. These results were confirmed in human resection specimens. The labeling of TAMs likely occurs because these cells also express high levels of cathepsins (43). The intraoperative identification of TAMs may, in fact, be beneficial to patients because TAMs tend to localize at the invasive front (or "margin") of the tumors (44, 45). Labeling of both TAMs and malignant cells by VGT-309 can thus aid surgeons' evaluation of whether a tumor resection margin is adequate to prevent locoregional tumor recurrence.

This study represents a significant advance in the field of fluorescence-guided surgery as the first to demonstrate successful human translation of a qABP for guiding resection of cancer in real time. A major weakness of the field of fluorescence-guided surgery—and molecular cancer research, more generally—is the overreliance upon preclinical testing of probes in tumors derived from cell lines that are monolithically positive for the molecular target of interest. These models do not recapitulate the enormous variation in gene expression, protein expression, and mutated protein expression within human tumors (4, 46). Here, we not only demonstrate highly specific tumor labeling in xenograft models, but also

show excellent tumor discrimination when VGT-309 was tested in spontaneously occurring canine and human tumors.

The preliminary data from our pilot human study of VGT-309 suggest the clinical promise of VGT-309 for improving the surgical management of patients with resectable tumors. In 1 patient, we found that VGT-309 localized a pulmonary tumor that was indistinguishable from normal lung parenchyma by visual inspection or palpation. This allowed removal of the lesion by a small wedge resection, rather than conversion to open thoracotomy or a large wedge resection, which would have involved removal of a substantial amount of normal lung parenchyma in a patient with compromised baseline pulmonary function. In the detection of visually occult or non-palpable disease, VGT-309–guided tumor resection has the potential to improve the completeness of cancer resection and thereby improve rates of post-operative recurrence and survival. Our study specifically concerned resection of pulmonary tumors as a proof-of-principle study, but the results are likely generalizable to a broad range of solid tumors given their demonstrated cathepsin overexpression.

This study adds to the field of fluorescence-guided surgery by showing successful clinical translation of a tumor-targeted, cathepsin activity–based probe that produces light in the NIR spectrum. Further studies are in progress to validate the utility of this technology in resection of human lung cancers. Additional trials in other tumor types are needed to more fully characterize the benefits and limitations of VGT-309, particularly in cancers of the thymus, kidneys, spleen, or liver, which are known to have cathepsin expression in normal parenchyma. Nonetheless, there is clear clinical promise of VGT-309 to localize cancer during surgery, potentially reducing the need for re-resection, lowering the rates of local recurrence, and personalizing adjuvant therapy.

Authors' Disclosures

G.T. Kennedy reports grants from Foundation for the NIH and American Philosophical Society during the conduct of the study. N.T. Sullivan reports grants from NIH T32 CA009140 during the conduct of the study. E. Bensen reports personal fees from Vergent Bioscience, Inc. during the conduct of the study, as well as personal fees and nonfinancial support from Vergent Bioscience, Inc. outside the submitted work; in addition, E. Bensen has a patent for 63/306,032 pending and licensed to Vergent Bioscience, Inc. and a patent for 63/306,019 pending and licensed to Vergent Bioscience, Inc. E. Bensen is an employee of Vergent Bioscience, Inc. receiving both a salary and equity in the company. Vergent sponsored the Phase I clinical trial at Nucleus Network and the Phase II trial at St Vincent's Hospital. Results from both of these trials are presented in the manuscript. Vergent provided VGT-309 free of charge for preclinical studies conducted at the University of Pennsylvania that are presented in this manuscript. J.T. Santini Jr reports personal fees from Vergent Bioscience, Inc. during the conduct of the study, as well as personal fees and nonfinancial support from Vergent Bioscience, Inc. outside the submitted work; in addition, J.T. Santini Jr has a patent for 63/306,032 pending and licensed to Vergent Bioscience, Inc. and a patent for 63/306,019 pending and licensed to Vergent Bioscience, Inc. J.T. Santini Jr is an employee of Vergent Bioscience, Inc. and owns equity in the company. M. Bogyo reports personal fees from Vergent Biosciences during the conduct of the study, as well as personal fees from Vergent Biosciences outside the submitted work; in addition, M. Bogyo has a patent for PCT licensed to Vergent Biosciences. J.D. Lickliter reports other support from Vergent Bioscience during the conduct of the study, as well as personal fees from Amplia Therapeutics and Ena Therapeutics outside the submitted work. G. Wright previously attended scientific meeting sponsored by Stryker, a company involved in near-infrared imaging technology. Stryker also provided G. Wright's institution with the near-infrared imaging equipment for the purpose of being used in the human study; no payments were made to G. Wright personally. No disclosures were reported by the other authors.

Authors' Contributions

G.T. Kennedy: Conceptualization, resources, data curation, formal analysis, funding acquisition, investigation, methodology, writing–original draft, writing–review and editing. **D.E. Holt:** Resources, data curation, formal analysis, investigation, writing–review and editing. **F.S. Azari:** Formal analysis, investigation, writing–review and editing. **E. Bernstein:** Data curation, formal analysis, investigation, writing–review and editing. **B. Nadeem:** Data curation, formal analysis, investigation, writing–review and editing. **A. Chang:** Data curation, formal analysis, investigation, writing–review and editing. **N.T. Sullivan:** Data curation, investigation, writing–review and editing. **A. Segil:** Data curation, investigation, writing–review and editing. **C. Deshpande:** Data curation, formal analysis, writing–review and editing. **E. Bensen:** Resources, investigation, writing–review and editing. **J.T. Santini Jr.:** Resources, investigation, writing–review and editing. **J.C. Kucharczuk:** Formal analysis, investigation, writing–review and editing. **E.J. Delikatny:** Resources, investigation, writing–review and editing. **M. Bogyo:** Resources, methodology, writing–review and editing. **A.J.M. Egan:** Resources, data curation, investigation, writing–review and editing. **C.W. Bradley:** Resources, data curation, writing–review and editing. **E. Eruslanov:** Formal analysis, methodology, writing–review and editing. **J.D. Lickliter:** Data curation, formal analysis, supervision, investigation, writing–review and editing. **G. Wright:** Resources, data curation, formal analysis, supervision, investigation, writing–review and editing. **S. Singhal:** Conceptualization, resources, formal analysis, supervision, funding acquisition, writing–original draft, writing–review and editing.

Acknowledgments

This study was supported by NIH grants F32CA254210 (to G.T. Kennedy), T32CA009140 (to N.T. Sullivan), and P01CA254859 (to S. Singhal). G.T. Kennedy was also supported by the American Philosophical Society via the Daland Fellowship in Clinical Investigation. F.S. Azari was supported by the Thoracic Surgery Foundation. G. Wright was supported by the VCCC Alliance funded by the Victorian Government. S. Singhal was also supported by the State of Pennsylvania Health Research Formula Fund.

The costs of publication of this article were defrayed in part by the payment of page charges. This article must therefore be hereby marked *advertisement* in accordance with 18 U.S.C. Section 1734 solely to indicate this fact.

Note

Supplementary data for this article are available at Clinical Cancer Research Online (http://clincancerres.aacrjournals.org/).

Received April 14, 2022; revised June 2, 2022; accepted July 1, 2022; published first July 6, 2022.

References

1. Aliperti LA, Predina JD, Vachani A, Singhal S. Local and systemic recurrence is the Achilles heel of cancer surgery. Ann Surg Oncol 2011;18:603–7.
2. Lauwerends LJ, Van Driel PBAA, Baatenburg De Jong RJ, Hardillo JAU, Koljenovic S, Puppels G, et al. Real-time fluorescence imaging in intraoperative decision making for cancer surgery. Lancet Oncol 2021;22:e186–95.
3. Garland M, Yim JJ, Bogyo M. A bright future for precision medicine: advances in fluorescent chemical probe design and their clinical application. Cell Chem Biol 2016;23:122–36.
4. Pogue BW, Rosenthal EL, Achilefu S, van Dam GM. Perspective review of what is needed for molecular-specific fluorescence-guided surgery. J Biomed Opt 2018;23:1–9.
5. Hernot S, Van Manen L, Debie P, Mieog JSD, Vahrmeijer AL. Latest developments in molecular tracers for fluorescence image-guided cancer surgery. Lancet Oncol 2019;20:e354–67.
6. Voskuil FJ, Steinkamp PJ, Zhao T, Van Der Vegt B, Koller M, Doff JJ, et al. Exploiting metabolic acidosis in solid cancers using a tumor-agnostic pH-activatable nanoprobe for fluorescence-guided surgery. Nat Commun 2020;11:3257.
7. Scott JI, Deng Q, Vendrell M. Near-infrared fluorescent probes for the detection of cancer-associated proteases. ACS Chem Biol 2021;16:1304–17.
8. Widen JC, Tholen M, Yim JJ, Antaris A, Casey KM, Rogalla S, et al. AND-gate contrast agents for enhanced fluorescence-guided surgery. Nat Biomed Eng 2021;5:264–77.

9. Hao L, Rohani N, Zhao RT, Pulver EM, Mak H, Kelada OJ, et al. Microenvironment-triggered multimodal precision diagnostics. Nat Mater 2021;20:1440–8.
10. Blum G, Mullins SR, Keren K, Fonovic M, Jedeszko C, Rice MJ, et al. Dynamic imaging of protease activity with fluorescently quenched activity–based probes. Nat Chem Biol 2005;1:203–9.
11. Berger AB, Vitorino PM, Bogyo M. Activity-based protein profiling: applications to biomarker discovery, in vivo imaging and drug discovery. Am J Pharmacogenomics 2004;4:371–81.
12. Blum G, Von Degenfeld G, Merchant MJ, Blau HM, Bogyo M. Noninvasive optical imaging of cysteine protease activity using fluorescently quenched activity–based probes. Nat Chem Biol 2007;3:668–77.
13. Olson OC, Joyce JA. Cysteine cathepsin proteases: Regulators of cancer progression and therapeutic response. Nat Rev Cancer 2015;15:712–29.
14. Palermo C, Joyce JA. Cysteine cathepsin proteases as pharmacologic targets in cancer. Trends Pharmacol Sci 2008;29:22–28.
15. Joyce JA, Baruch A, Chehade K, Meyer-Morse N, Giraudo E, Tsai F-Y, et al. Cathepsin cysteine proteases are effectors of invasive growth and angiogenesis during multistage tumorigenesis. Cancer Cell 2004;5:443–53.
16. Verdoes M, Oresic Bender K, Segal E, Van Der Linden WA, Syed S, Withana NP, et al. Improved quenched fluorescent probe for imaging of cysteine cathepsin activity. J Am Chem Soc 2013;135:14726–30.
17. Suurs FV, Qiu S-Q, Yim JJ, Schrā Der CP, Timmer-Bosscha H, Bensen ES, et al. Fluorescent image-guided surgery in breast cancer by intravenous application of a quenched fluorescence activity–based probe for cysteine cathepsins in a syngeneic mouse model. EJNMMI Res 2020;10:111.
18. Chauhan SS, Goldstein LJ, Gottesman MM. Expression of cathepsin L in human tumors. Cancer Res 1991;51:1478–81.
19. Gal S, Gottesman MM. Isolation and sequence of a cDNA for human pro-(cathepsin L). Biochem J 1988;253:303–6.
20. Liu X, Yue P, Zhou Z, Khuri FR, Sun S-Y. Death receptor regulation and celecoxib-induced apoptosis in human lung cancer cells. J Natl Cancer Inst 2004;96:1769–80.
21. Edgington-Mitchell LE, Bogyo M, Verdoes M. Live cell imaging and profiling of cysteine cathepsin activity using a quenched activity–based probe. Methods Mol Biol 2017;1491:145–59.
22. Kennedy GT, Azari FS, Bernstein E, Nadeem B, Chang AE, Segil A, et al. A prostate specific membrane antigen-targeted near-infrared conjugate for identifying pulmonary squamous cell carcinoma during resection. (Image-guided resection of pulmonary squamous cell carcinoma). Mol Cancer Ther 2022;21:546–54.
23. Freireich EJ, Gehan EA, Rall DP, Schmidt LH, Skipper HE. Quantitative comparison of toxicity of anticancer agents in mouse, rat, hamster, dog, monkey, and man. Cancer Chemother Rep 1966;50:219–44.
24. Leblanc AK, Mazcko CN. Improving human cancer therapy through the evaluation of pet dogs. Nat Rev Cancer 2020;20:727–42.
25. Kennedy GT, Azari FS, Bernstein E, Desphande C, Din A, Marfatia I, et al. 3D specimen mapping expedites frozen section diagnosis of non-palpable ground glass opacities. Ann Thorac Surg 2021;S0003-4975(21)01848-8.
26. Predina JD, Newton AD, Connolly C, Dunbar A, Baldassari M, Deshpande C, et al. Identification of a folate receptor–targeted near-infrared molecular contrast agent to localize pulmonary adenocarcinomas. Mol Ther 2018;26:390–403.
27. Kominami E, Tsukahara T, Bando Y, Katunuma N. Distribution of cathepsins B and H in rat tissues and peripheral blood cells. J Biochem 1985;98:87–93.
28. Verdoes M, Edgington LE, Scheeren FA, Leyva M, Blum G, Weiskopf K, et al. A nonpeptidic cathepsin S activity–based probe for noninvasive optical imaging of tumor-associated macrophages. Chem Biol 2012;19:619–28.
29. Dijkstra BM, De Jong M, Stroet MCM, Andreae F, Dulfer SE, Everts M, et al. Evaluation of ac-Lys0 (IRDye800CW) Tyr3-octreotate as a novel tracer for SSTR2-targeted molecular fluorescence guided surgery in meningioma. J Neurooncol 2021;153:211–22.
30. Walker E, Liu Y, Kim I, Biro M, Iyer SR, Ezaldein H, et al. A protease-activated fluorescent probe allows rapid visualization of keratinocyte carcinoma during excision. Cancer Res 2020;80:2045–55.
31. Yim JJ, Harmsen S, Flisikowski K, Flisikowska T, Namkoong H, Garland M, et al. A protease-activated, near-infrared fluorescent probe for early endoscopic detection of premalignant gastrointestinal lesions. Proc Natl Acad Sci USA 2021;118:e2008072118.
32. Habibollahi P, Figueiredo J-L, Heidari P, Dulak AM, Imamura Y, Bass AJ, et al. Optical imaging with a cathepsin B activated probe for the enhanced detection of esophageal adenocarcinoma by dual channel fluorescent upper GI endoscopy. Theranostics 2012;2:227–34.
33. Whitley MJ, Cardona DM, Lazarides AL, Spasojevic I, Ferrer JM, Cahill J, et al. A mouse-human phase I co-clinical trial of a protease-activated fluorescent probe for imaging cancer. Sci Transl Med 2016;8:320ra4.
34. Lanahan CR, Kelly BN, Gadd MA, Specht MC, Brown CL, Hughes KS, et al. Performance of a novel protease-activated fluorescent imaging system for intraoperative detection of residual breast cancer during breast conserving surgery. Breast Cancer Res Treat 2021;187:145–53.
35. Smith BL, Gadd MA, Lanahan CR, Rai U, Tang R, Rice-Stitt T, et al. Real-time, intraoperative detection of residual breast cancer in lumpectomy cavity walls using a novel cathepsin-activated fluorescent imaging system. Breast Cancer Res Treat 2018;171:413–20.
36. Yim JJ, Tholen M, Klaassen A, Sorger J, Bogyo M. Optimization of a protease activated probe for optical surgical navigation. Mol Pharm 2018;15:750–8.
37. Ofori LO, Withana NP, Prestwood TR, Verdoes M, Brady JJ, Winslow MM, et al. Design of protease activated optical contrast agents that exploit a latent lysosomotropic effect for use in fluorescence-guided surgery. ACS Chem Biol 2015;10:1977–88.
38. Kennedy GT, Azari F, Nadeem B, Chang A, Segil A, Bernstein E, et al. 500 consecutive pulmonary resections guided by intraoperative molecular imaging: Lessons from a single institutional experience. Abstract presented at the Annual Meeting of the American Surgical Association. Chicago, IL. April 9, 2022.
39. Randall LM, Wenham RM, Low PS, Dowdy SC, Tanyi JL. A phase II, multicenter, open-label trial of OTL38 injection for the intraoperative imaging of folate receptor-alpha positive ovarian cancer. Gynecol Oncol 2019;155:63–68.
40. Predina JD, Newton AD, Keating J, Dunbar A, Connolly C, Baldassari M, et al. A phase I clinical trial of targeted intraoperative molecular imaging for pulmonary adenocarcinomas. Ann Thorac Surg 2018;105:901–8.
41. Gangadharan S, Sarkaria I, Rice D, Murthy S, Braun J, Kucharczuk J, et al. Multi-institutional phase II clinical trial of intraoperative molecular imaging of lung cancer. Ann Thorac Surg 2021;112:1150–9.
42. Kennedy GT, Azari FS, Bernstein E, Marfatia I, Din A, Kucharczuk JC, et al. Targeted intraoperative molecular imaging for localizing non-palpable tumors and quantifying resection margin distances. JAMA Surg 2021;156:1043–50.
43. Quillard T, Croce K, Jaffer F, Weissleder R, Libby P. Molecular imaging of macrophage protease activity in cardiovascular inflammation *in vivo*. Thromb Haemost 2011;105:828–36.
44. König L, Mairinger FD, Hoffmann O, Bittner A-K, Schmid KW, Kimmig R, et al. Dissimilar patterns of tumor-infiltrating immune cells at the invasive tumor front and tumor center are associated with response to neoadjuvant chemotherapy in primary breast cancer. BMC Cancer 2019;19:120.
45. Pollard JW. Macrophages define the invasive microenvironment in breast cancer. J Leukoc Biol 2008;84:623–30.
46. Azari F, Kennedy G, Bernstein E, Hadjipanayis C, Vahrmeijer AL, Smith BL, et al. Intraoperative molecular imaging clinical trials: a review of 2020 conference proceedings. J Biomed Opt 2021;26:050901.